SPECTRAL BAND CHARACTERIZATION FOR HYPERSPECTRAL MONITORING OF WATER QUALITY

Stephanie C. Vermillion,[†] Rolando Raqueño,[‡] Rulon Simmons[†]

1. INTRODUCTION

1.1 Motivation

A method for selecting the set of spectral characteristics that provides the smallest increase in prediction error is of interest to those using hyperspectral imaging (HSI) to monitor water quality. The spectral characteristics of interest to these applications are spectral bandwidth and location. Three water quality constituents of interest that are detectable via remote sensing are chlorophyll (CHL), total suspended solids (TSS), and colored dissolved organic matter (CDOM). Hyperspectral data provides a rich source of information regarding the content and composition of these materials, but often provides more data than an analyst can manage. This study addresses the spectral characteristics need for water quality monitoring for two reasons. First, determination of the greatest contribution of these spectral characteristics would greatly improve computational ease and efficiency. Second, understanding the spectral capabilities of different spectral resolutions and specific regions is an essential part of future system development and characterization. As new systems are developed and tested, water quality managers will be asked to determine sensor specifications that provide the most accurate and efficient water quality measurements. We address these issues using data from AVIRIS and a set of models to predict constituent concentrations.

1.2 Background

Hyperspectral data has been used for a number of applications including geology, vegetation mapping, and atmospherics. We believe that hyperspectral imaging holds the potential for remotely monitoring important water quality constituents. This area has previously received little attention compared to the other applications listed above. Water quality monitoring is an important issue for communities everywhere. There is a myriad of agencies at the local, state, national, and international levels actively involved in this issue. Monitoring concerns range from phosphorous to organic sediments and animal water run-off. Water quality monitoring is an area where a significant amount of conventional and surface surveying and monitoring work has already taken place. Furthermore, an area could greatly benefit from improved information regarding where to take a reduced set of local field samples and a means to interpolate and extrapolate results over a much larger study area. Thus, HSI is seen as a cost-effective solution for surveying water quality over large areas.

1.3 Proposed Contribution

This study performs two minimization studies using 30 AVIRIS bands, ranging from 419nm to 683nm. First, a band averaging method is used to determine the maximum bandwidth obtainable with no significant increase in constituent prediction accuracy. Spectrally degraded AVIRIS bands were used with the prediction models to show error as compared to field measurements. Results are presented based on the prediction error degraded resolution provides when compared to the 30-band AVIRIS data. Second, a principal component analysis is used to rank modeled reflectance values at each AVIRIS bandpass according to their correlation with the first principal component. The method then tracks the error between the constituent components predicted using the ranked bands and field measurements. The results of the study show the error in prediction as a function of the number of bands, given the chosen rank ordering.

2 METHODOLOGY

2.1 Simulation Tools

HydroMod is a computer-aided tool that models the complex radiometry of aquatic systems including the impact from clouds, wind speed, and the scattering characteristics of water. This model builds upon past work by Bukata *et al*. (1995) and ongoing work at RIT to link bio-optical models of air-water interface models and atmospheric radiative transfer models (Berk, 1989). HydroMod is used with the HydroLight water radiance propagation model (Mobley, 1994) to simulate water-leaving spectral radiance above and below the water's surface for varying values of water quality parameters. Spectral measurements can then be compared with this family of predicted water-leaving spectral radiance output to find the best match and subsequently the associated water quality

[†] Eastman Kodak Company (stephanie.vermillion@kodak.com)
[‡] Rochester Institute of Technology

parameters used to generate the matching. The optimization algorithm that was used is a downhill simplex algorithm called *AMOEBA* (Press, 1992).

2.2 Test Data

The AMOEBA algorithm requires two inputs to create the constituent concentration maps: a library of constituent spectra and an image to classify. For this study, the signature library used is a HydroMod look-up-table (LUT) that contained 640 spectral signatures. The 640 signatures were created using between eight and ten different concentration levels of each constituent and all of their combinations. The water quality constituents are measured in units of scalar carbon[1] (CDOM), mg/m^3 (CHL), and g/m^3 (TSS). The LUT available for this study was generated with more samples at lower concentration levels to best represent the sampling needs of the littoral coastal environment. In order to make the results of this study applicable to multiple environments, an even sampling of all concentrations is required. To estimate the spectrum of any combination of constituents not specifically specified in the original LUT, a piecewise trilinear interpolation is used. The interpolation selects the closest fit for the desired spectrum by interpolating simultaneously over each of the three water constituent's reflectance values. Table 1 shows the concentration levels used in this study and the values contained in the original 640 signature library. The input images were band subsets of a 30-band (419-683nm) reflectance calibrated AVIRIS image. Reflectance calibration was performed using a three point Empirical Line Method (ELM).

Table 1. Listing of the constituent concentrations used for this study and the LUT values from which they were interpolated. Study concentrations were selected by fixing the start and end values and dividing the remaining range evenly to create ten equally spaced levels.

Constituent	LUT Concentrations (8-10 Uneven Levels)	Study Concentrations (10 Even Levels)
CDOM	0.0, 0.015, 0.030, 0.145, 0.550, 2.0, 8.0, 30.0	0, 3.33, 6.66, 9.99, 13.32, 16.65, 19.98, 23.31, 26.64, 30
TSS	0.0, 0.015, 0.030, 0.145, 0.550, 2.0, 8.0, 30.0	0, 3.33, 6.66, 9.99, 13.32, 16.65, 19.98, 23.31, 26.64, 30
CHL	0.0, 0.03, 0.30, 0.525, 0.750, 2.0, 5.0, 13.0, 85.0, 33.0	0, 9.44, 18.88, 28.32, 37.76, 47.2, 56.64, 66.08, 75.52, 85

2.3 Band Averaging

The narrowest bands obtainable may not be the best choice for all remote-sensing applications. Broader bandwidths provide the sensor the capability to collect more photons, increasing the signal to noise ratio. Spectral signatures for detectable targets vary greatly within a class. Some of those variations may have a low frequency of spectral change. If the signatures are "smooth," then coarser resolutions (broader bands) will provide sufficient information as finer resolutions, with minimal addition of noise. Determining the widest bandwidth possible for the measurement of water quality constituents is needed to provide the most efficient means of data collection.

An understanding of the bandwidth requirements needed for accurate water quality measurements can be determined by analyzing adjacent bands. We explored coarser data sets by averaging the AVIRIS data (9nm channels). We selected new bandwidths by dividing the range of the 30-band data by the number of new bands. New band centers are designated by the wavelength value halfway between the average bandwidth and the initial wavelength (419nm). Additional bands are then evenly spaced based on the average bandwidth. The AMOEBA algorithm error for each of these new data sets is then calculated with respect to the original 30-band data (Table 2). Error is measured by calculating the root mean square (RMS) error between each simulated data map and the 30 band "truth" maps.

2.4 Band Selection

Ideally, a band selection study consists of an examination of all possible band combinations and their interactions effects. Given the high dimensionality of hyperspectral data, a thorough search for spectral uniqueness would be a substantial computational effort. The spectral richness of hyperspectral data further complicates analysis due to the high correlation of the bands. Often conclusive statistical decisions are unobtainable because it is difficult

[1]NOTE: Because the presence of CDOM cannot be directly detected by the hyperspectral sensor, measurements must be related to the absorption curve as a proportional indicator, and all other concentrations were scaled to that curve.

Table 2. Bandwidths used for the study (all fall within 419-683nm).

Number of Spectral Bands	Bandwidth
30	9nm
25	11nm
20	13nm
15	18nm
10	27nm
5	53nm

to select obvious thresholds or determine significant differences. Transforming hyperspectral data to a lower dimensional space addresses each of these issues.

We propose a method that determines the minimum number of bands needed for water quality measurements based on a Principal Component Analysis (PCA) and an error minimization process. PCA is commonly used in remote sensing as a data reduction technique. A PCA involves transforming the raw sensor data into a new space of uncorrelated components with certain ordered variance properties (Singh and Harrison, 1985). Our PCA method follows the steps proposed by Short (1982) and uses the spectral statistics from the HydroMod predicted reflectance.

The process of the PCA begins with the decomposition of the covariance matrix, **K**, of the concentration reflectance values according to

$$\mathbf{K} = (\mathbf{E}^{\mathbf{T}})^{-1}\mathbf{\Lambda}\mathbf{E}^{-1} \equiv \{\mathbf{k}_{ij}\}$$

where $\mathbf{\Lambda}$ = diag { $\lambda_1,\lambda_2, \ldots\lambda_n$ } contains the N eigenvalues of **K**, **E** holds the eigenvectors associated with $\lambda_1,\ldots\lambda_n$, and N represents the number of hyperspectral bands. Specifically, $\mathbf{E} = \{\mathbf{e}_{ij}\} = \left[\mathbf{e}_1 \vdots \mathbf{e}_2 \vdots \cdots \vdots \mathbf{e}_{\mathbf{N}}\right]$, where $\mathbf{e}_{ij}$ is the contribution of band *i* to component *j*.

The eigenvalues can be used to calculate the percent of total variance explained by each component *j* using Equation 1. Usually, the first transformed component describes the majority (over 80%) of the spectral variability in a data set (Jensen, 1996). We propose that bands with the highest contribution to the first principal component will be the most valuable as spectral input to the AMOEBA algorithm.

$$\text{Percent of variance described} = \frac{100\lambda_{\mathbf{i}}}{\mathbf{tr}(\mathbf{K})^{\mathbf{T}}} \qquad \text{(Equation 1)}$$

The contribution of each spectral band to the first component is determined using Equation 2. The band "loading" is calculated by computing the correlation between each band and each component. The loading values from the original data can then be used to rank each band's importance to the first component, and subsequently their importance to the AMOEBA algorithm. The loading of band *i* unto the j_{th} principal component is

$$\beta_{ij} = \mathbf{e}_{ij}\,[(\lambda_i)/(\mathbf{k}_{ij})]^{1/2} \qquad \text{(Equation 2)}$$

Our error minimization process incorporates the information gained from the band ranking as established by their loading to the first component. Once the band ranking is determined, band subsets are tested for prediction accuracy. We begin with the 30-band image and create 29 new band subsets, each time eliminating the band with the lowest ranking. Removal of the least valuable band for every trial allows for tracking of the prediction error through the band rankings. Next, we input each band subset into the AMOEBA algorithm, resulting in 29 error measurements. The single band subset can not be tested because the AMOEBA algorithm requires at least two points to make a concentration prediction. A reference data set is available for 11 points in the AVIRIS scene. At each reference point, we collected water samples (constituent concentrations), geo-location data, and field spectrometer reflectance measurements. We calculated the root-mean-square (RMS) error between the concentration trials and the 11 field measurements and averaged samples to provide one RMS value. This error measurement is used to indicate which bands between 400-700nm are the most useful for hyperspectral water quality monitoring. Because this method of analysis considers all three constituents simultaneously, the RMS results for each of the constituents was averaged to provide a total prediction error.

3. EXPERIMENTAL RESULTS

3.1 Band Averaging

The RMS error for each simulated data set verses the 30-band "truth" images is listed in Table 3. The control error was calculated by running the AMOEBA algorithm on the LUT spectra (instead of the pixel reflectance) and comparing those results to the known LUT concentrations. This provides a reference for the analysis of error for the band-simulated data sets. Figures 1-3 have been provided to better visualize the trends in the error by constituent.

Table 3. RMS Error for the averaged band simulated data sets.

Number of Bands	CHL	TSS	CDOM
5	4.43	1.40	3.29
10	2.81	0.48	1.50
15	2.32	0.37	1.25
20	1.90	0.33	1.09
25	1.93	0.34	1.12

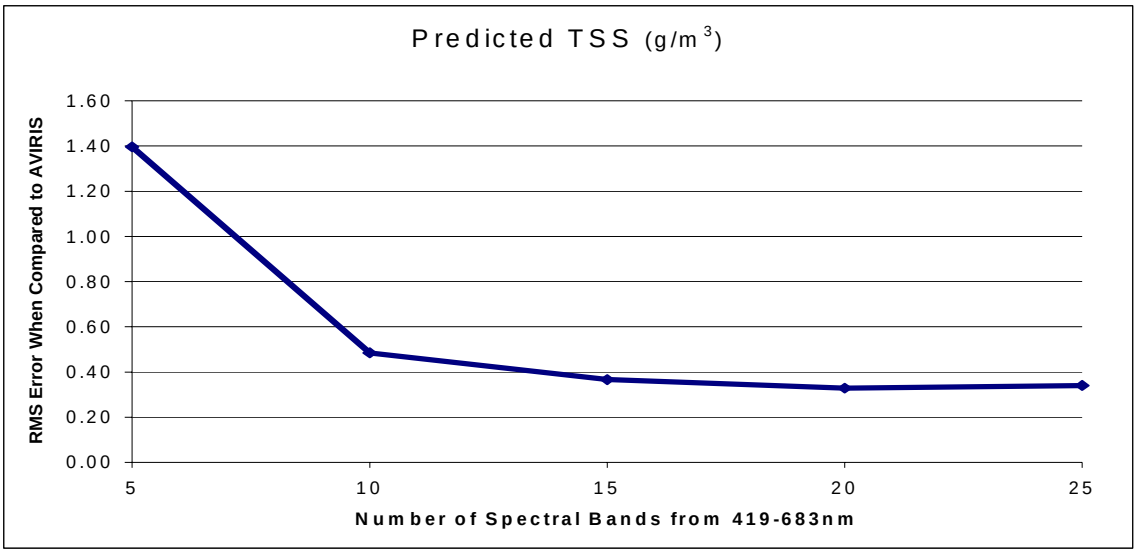

Figure 1. Plot of the RMS error between 30-band AMOEBA results and the spectrally degraded simulated images for TSS.

For all water constituents, as spectral resolution decreases, the algorithm error increases. There does not appear to be a significant change in the error for any of the constituents between 20 and 25 spectral bands. Using this method, analysts may choose to use as few as 15 bands, with errors comparable to 0.37 g/m^3 (TSS), 1.25 scalar carbon (CDOM), and 2.32 mg/m^3 (CHL). TSS was the least affected by changes in spectral resolution, having the smallest error between resolutions ($\bar{x}$ = 0.26) as well as the smallest range of error (1.07). The error ranges for CDOM and CHL were 2.19 and 2.52 respectively.

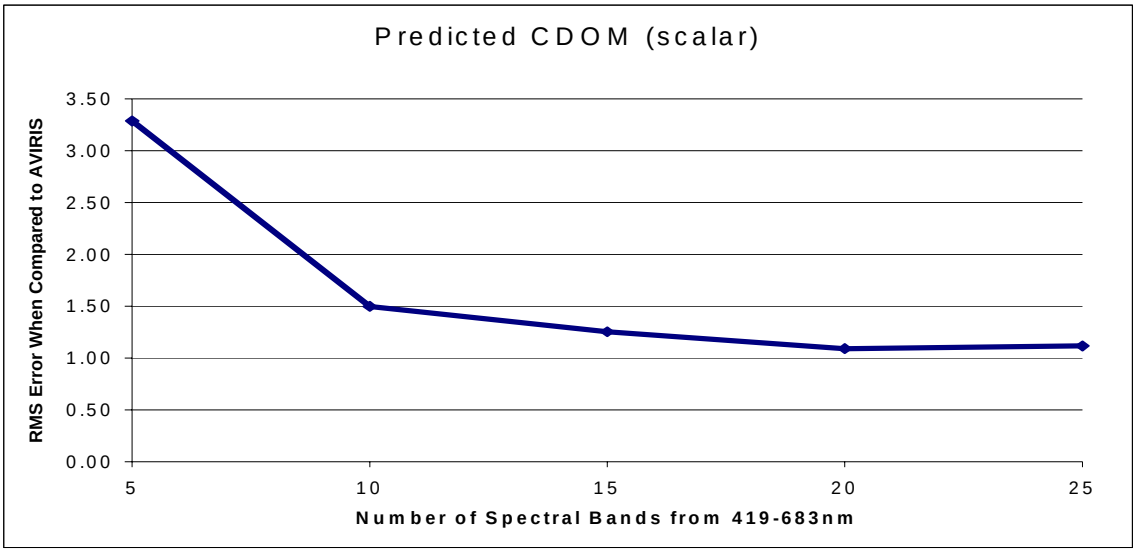

Figure 2. Plot of the RMS error between 30-band AMOEBA results and the spectrally degraded simulated images for CDOM.

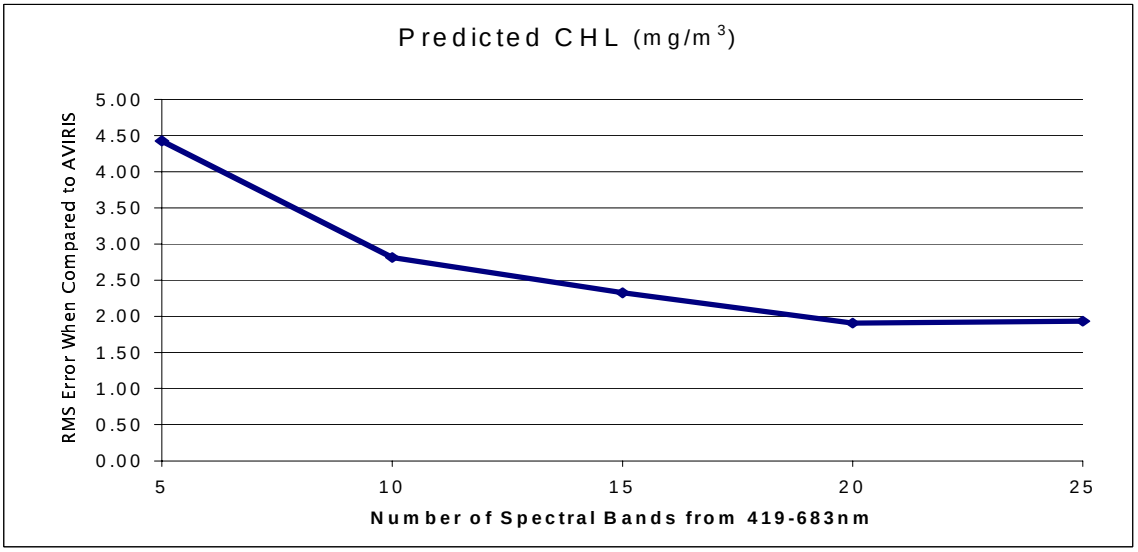

Figure 3. Plot of the RMS error between 30-band AMOEBA results and the spectrally degraded simulated images for CHL.

3.2 Band Selection

A PCA was used to transform the 30-band modeled reflectance data. The first principal component accounted for 89.68% of the spectral variance in the data set. Components 2 and 3 accounted for and additional 10% of the variance, and the components greater than three provided mostly noise. A list of the entire band loading is provided in Table 4. The highest band loading for the first component were for bands 5,10, and 4 (6.20, 3.55, and 3.38 respectively). The lowest loading was from bands 21 (0.25), 30 (0.15), and 28 (0.14). This indicates that the blue region (400-500nm) may be contributing the most to the variance in the data set. The red region (600-700nm) bands are contributing the least to the data set variance.

Table 4. Band loading for the first principle component of the 30 band transformed image.

Band Ranking	Band Number	Wavelength	Loading		Band Ranking	Band Number	Wavelength	Loading
1	5	439.63	6.1983		16	23	616.42	0.9266
2	10	488.74	3.5467		17	27	655.71	0.9242
3	4	429.81	3.3780		18	1	400.35	0.8184
4	9	478.92	3.0948		19	13	518.20	0.7565
5	7	459.27	2.7986		20	24	626.24	0.7070
6	8	469.10	2.4987		21	14	528.02	0.6485
7	12	508.38	2.2926		22	3	419.99	0.6365
8	11	498.56	2.2885		23	20	586.95	0.5556
9	15	537.85	1.9302		24	17	557.49	0.5293
10	2	410.17	1.7560		25	29	675.35	0.4588
11	19	577.13	1.5819		26	16	547.67	0.4160
12	6	449.45	1.4907		27	25	636.06	0.3142
13	26	645.88	1.0129		28	21	596.78	0.2454
14	22	606.60	0.9502		29	30	683.90	0.1517
15	18	567.31	0.9447		30	28	665.53	0.1371

The results of the band selection method are summarized in Figure 4. The overall error trend shows a decrease in prediction error as more bands are added. The error ranges from 4.09 to 37.84 with a minimum at 30 bands and a maximum at three bands. There are two substantial drops in the error, one at 12 bands and one at 23. Areas where there are large drops in error may indicate thresholds for the selection of the minimum number of bands required for water quality monitoring. To make the best decision as to the bands to select, an understanding of these three error regions is essential. It is important to note that although the individual constituent errors assist with the analysis of this study, the objective was to provide a recommendation for the best bands to predict all three constituents simultaneously.

The bands loading the variance the most are the first 11 bands in the ranking (see Table 3). Upon individual examination of those bands, we see that the TSS average spectrum has a much higher reflectance than both the CHL and the CDOM. This may be why the error using the first 11 bands is low for TSS, and higher for CDOM and CHL (Figure 5). More specifically, the 11 bands being used by the AMOEBA algorithm are the bands that provide the best fit for TSS spectra, not necessarily the best fit for CDOM and CHL (increasing the individual errors).

The next region of interest is between the bands ranked 12 to 22. These bands are ranked higher because the variance among all three constituents is high. When the 12th band is added to the first 11, the individual errors for CDOM and CHL demonstrate opposite trends. At this band, the CDOM error drops considerably (61.84 units) and the CHL error increases 7.47 units. The CHL error continues to fluctuate and rise to a maximum of 36.10. This increase in the CHL error may be due to reflectance confusion between the CHL and TSS data. After 550nm, CHL and TSS exhibit similar average spectral curves. An examination of the reflectance curves for both constituents shows an overlapping of values as the concentrations change. Although the TSS signatures dominated the first 11 bands, all three constituents were separable. For this region, the algorithm has difficulty fitting CHL pixel values because it may not be able to separate a low concentration of TSS from a high concentration of CHL. The CDOM error improves here because it is not confused with TSS or CHL. The TSS error is unchanged most likely because it is still weighting the variance more then the CHL spectra.

The third region of interest is the bands ranked greater than 22. This region is created when the error drops significantly at the band ranked 23. This effect is related to the confusion described in the previous section. The bands ranked 23-25 provide improved error for the CHL spectra. At those bands, the variance from the CHL spectra becomes separable enough from the TSS spectra that the algorithm can provide a better spectral fit. Two of these bands fall within the algorithm weighting region of CHL, and one (683nm) falls where there is little spectral overlap between CHL and TSS.

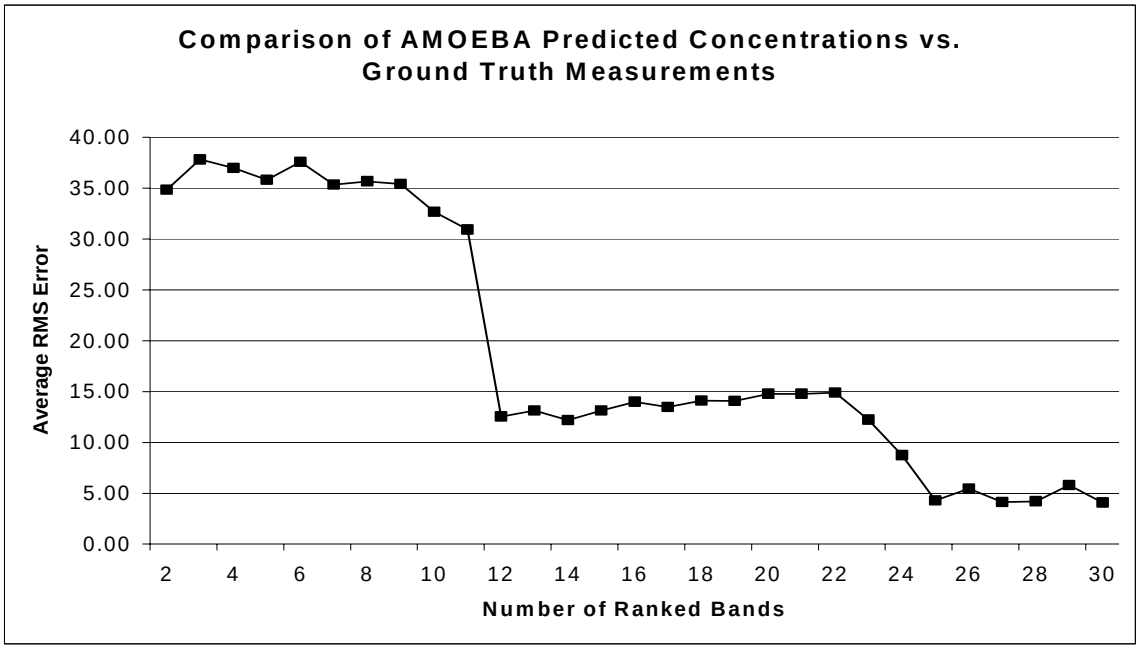

Figure 4. Plot of the average RMS error between AMOEBA predicted concentrations and ground truth measurements for all three constituents.

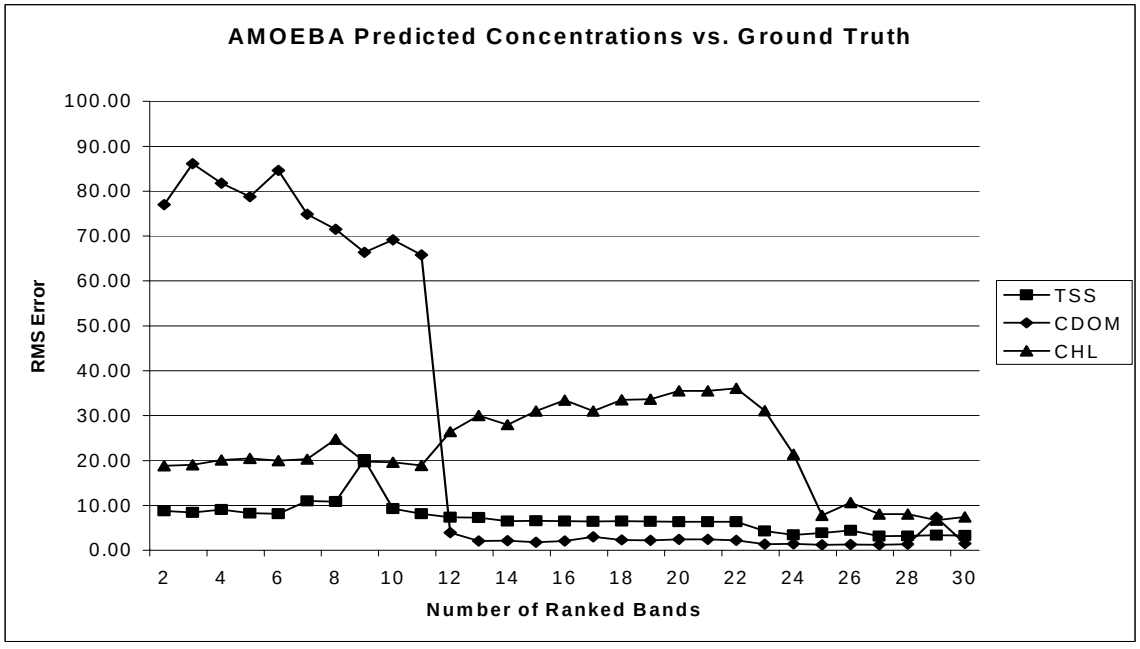

Figure 5. Plot of the average RMS error between AMOEBA predicted concentrations and ground truth measurements for all three constituents listed individually.

Given this understanding of the trends in prediction error, bands can be selected to reduce the raw data set with minimal addition of measurement error. The 30-band data set can be reduced to 23 bands with an error increase of 8.15 units for a total error of 12.24. Of primary interest, however, is the effect of reducing the data set to 12 bands. At the 12-band threshold, the total predicted error is 12.56 (an increase of 8.47 units). This error may be

well within the acceptable limit for some water quality applications. However, before the 12-band ranked subset can be recommended, the analysts must understand how the water quality information is being separated in this region.

Although the TSS signatures dominate the spectral variance in the first band region, this region can be used for the prediction of all three constituents together. This is because there is little overlap across the concentration range of all three constituents. Spectral overlap occurs between TSS and CHL for almost every concentration level, indicating that separation of these constituents may be difficult. However, how and to what degree these spectra are overlapping may contradict that assumption. CDOM is separable at all concentration levels from the other two constituents, and is not of concern for spectral overlap.

4. CONCLUSIONS AND FUTURE WORK

Given this optimization strategy, this study provides a set of 12 spectral bands that can be used for the prediction of water quality constituents with a RMS error of 12.56. This is an 8.47 unit error increase from using the maximum amount of data available across the 400-700nm spectral range. Of those 12 bands, nine fall within the blue spectral region (400-500nm) and 3 fall within the green range (500-600nm). Using the highest spectral resolution data currently available (AVIRIS), the best prediction error the AMOEBA algorithm provides is a RMS of 4.09. These are small units when considering the 20-meter sample pixel of AVIRIS. It does not seem likely that an error of +8 units will make a substantial difference when mapping water constituents over large areas. For most purposes, spectral data with 13nm channels (20 bands, 400-700nm) can be utilized with no significant addition of error. Analysts may chose data with 18nm bandwidths with some additional error; however, the impact of that error on water quality results will depend on the acceptable error associated with a specific task.

Although this is one of the better strategies for spectral characterization, we understand its limitations. First, PCA does not consider the spectral separability of the constituents. More specifically, it assumes that there is an even contribution from all of the constituents to the reflectance of the entire scene. This is rarely the case. Often one signature may have a much higher reflectance than the other components at the same band. For that band the variance will be biased towards the dominant signature. Another limitation of our method this that we have limited our analysis to the first principal component. Although that component describes the vast majority of the variance in the data set, there may be a significant contribution in the remaining components. Finally, our method uses models for our error measurements that are experimental in nature. It is important to note that determining the accuracy of the AMOEBA algorithm is beyond the scope of this study. A complete discussion of the simulation tools used for this study can be found in the final report for the NASA EOCAP contract NAS13-98080. The models used for this study are recently developed tools designed to fulfil an immediate need in the water quality community. Further refinement is required before they are fully implemented for water quality monitoring.

This study indicates that both the width and the placement of spectral bands are important to water quality monitoring. As new systems are developed and tested, water quality managers will be asked to determine sensor specifications that provide the most accurate and efficient water quality measurements. As studies such as this one develop, it may become clear that existing sensors may be adequate for water quality monitoring. If so, determining the best spectral characteristics becomes useful not only to increase computational ease, but also to assist with the sampling issues that plague the water quality community. Sensitivity studies similar to this one can provide an indication of the amount of error to be expected given varying spectral conditions. If hyperspectral data was not available given certain acquisition parameters (i.e., cloud cover), it may be acceptable to collect data from a broad band sensor given an understanding of the inherent error at that resolution. For example, animal water run-off measurements are often event-driven collections. If for some reason samples cannot be collected using one of the methods some other method may be better then no data at all. Understanding how the error in the prediction of water quality constituents is related to the spectral characteristics of remotely sensed data is a valuable reference for the water quality community.

To answer the question of required system specifications most accurately, a functional measure that is two-dimensional (width and location) in nature is required. This study was developed as part of a larger project to design and test hyperspectral algorithms for the monitoring of water quality. The resources were not available for an extensive joint minimization study, but future exploration of this topic is encouraged.

5. ACKNOWLEDGEMENTS

The work associated with this paper was funded under the NASA EOCAP project NAS-98080 and was completed co-jointly at the Eastman Kodak Company and the Rochester Institute of Technology in Rochester, NY. We thank Jim Coss and Jason Hamel for their assistance with data processing as well as Shiloh Dockstader and Mike Heath for their technical advisement and support.

6. REFERENCES

Berk, A., L.S. Bernstein, and D.C. Robertson, 1989, "MODTRAN: a moderate resolution model for LOWTRAN 7," GL-TR-89-0122, Spectral Science, Burlington, MA.

Bukata, R.P., J.H. Jerome, K.Ya. Krondratyev, and D.V. Pozdnyakov, 1995, "Optical Properties and Remote Sensing of Inland and Coastal Waters," New York: CRC Press, ISBN 0-8493-4754-8, 362 pages.

Jensen, J.R., 1996, "Introductory Digital Image Processing: A Remote Sensing Perspective," Upper Saddle River, NJ: Prentice Hall, ISBN 0-13-205840-5, pp. 172-179.

Mobley, C.D, 1994, "Light and Water: Radiative Transfer in Natural Waters," Boston, Academic Press, ISBN 0-12-502750-8, 592 pages.

Press, W.H., 1992, "Numerical Recipes in C: The Art of Scientific Computing," Cambridge University Press, pp. 408-412.

Short, N., 1982, "Principles of Computer Processing of Landsat Data," Appendix A in The Landsat Tutorial Workbook, Publication 1078. Washington: National Aeronautics and Space Administration, pp. 421-453.

Singh, A. and A. Harrison, 1985, "Standardized Principal Components," International Journal of Remote Sensing, vol. 6, pp. 883-896.